Supplementary Information (SI) for Inorganic Chemistry Frontiers.
This journal is © the Partner Organisations 2025

Investigating the Impact of Counter Anions on Electrocatalytic Alcohol Oxidation Reaction over MOF-derived Catalysts

Yining Li [a], Abhishek Dutta Chowdhury [a, *]

Chemical reagent. $Cu(NO_3)_2 \cdot 3H_2O$ (99 %, Innochem), $Cu(SO_4)_2 \cdot 5H_2O$ (99 %, Innochem), $CuCl_2$ (98 %, Energy Chemical), $Co(NO_3)_2 \cdot 6H_2O$ (99.99 %-Co, Xiangding), ethanol (EtOH, AR, Sinopharm), methanol (CH_3OH, AR, Sinopharm), N,N-Dimethylformamide (DMF, AR, Sinopharm), potassium hydroxide (KOH, AR, Sinopharm), carbon paper (100*100 mm, GaossUnion), deuterium oxide (D_2O, 99 % D, Energy Chemical), dimethyl sulfoxide (DMSO, 98 %, Energy Chemical). All the chemicals were used as received without further purification.

Synthesis of MOF-based electrocatalytic materials. As-synthesized MOF-based materials were labeled as Cu_xCo_y-BTC (where x and y are the molar ratios of copper and cobalt, respectively, BTC: H_3BTC). Cu_xCo_y-BTC materials' synthesis was inspired by the analogous report in the literature, including our previous work [1–5] . Typically, the amount of each metal salt as well as their weight used in the starting reaction mixture are: for $Cu_{0.4}Co_{0.6}$-BTC: $Cu(NO_3)_2 \cdot 3H_2O/Cu(SO_4)_2 \cdot 5H_2O/CuCl_2$ (0.66 mmol) and $Co(NO_3)_2 \cdot 6H_2O$ (1.00 mmol); for $Cu_{0.2}Co_{0.8}$-BTC: $Cu(SO_4)_2 \cdot 5H_2O$ (0.33 mmol) and $Co(NO_3)_2 \cdot 6H_2O$ (1.33 mmol); for $Cu_{0.1}Co_{0.9}$-BTC: $Cu(SO_4)_2 \cdot 5H_2O$ (0.17 mmol) and $Co(NO_3)_2 \cdot 6H_2O$ (1.49 mmol); for $Cu_{1.0}Co_0$-BTC: $Cu(SO_4)_2 \cdot 5H_2O$ (1.66 mmol); for $Cu_0Co_{1.0}$-BTC: $Co(NO_3)_2 \cdot 6H_2O$ (1.66mmol). The metallic precursor and H_3BTC (200 mg, 0.952 mmol) were mixed and dissolved in 12 ml DMF solvent in a vial. The vial was sealed and heated at 85 °C for 12 h to yield a blue precipitate of Cu_xCo_y-BTC materials. The unreacted H_3BTC inside the pores of MOF was removed by extensive solvent (DMF, EtOH) exchange and dried under the vacuum degassing station at 80°C for 6h under Ar in circulation.

Characterization. Powder X-ray diffraction (XRD) analysis was performed using a

Bruker D8 AD-VANCE X diffractometer (Bruker, Karlsruhe, Germany) using a Cu Kα radiation source ($\lambda = 0.154$ nm). Diffraction patterns are collected in the 2θ range between 0° and 90° with a step size of 3°/min. The catalysts' lattice constant and average grain size are analyzed using JADE software to analyze the recorded data. Scanning electron microscopy (SEM) images were acquired on a thermal field emission scanning electron microscope model Zeiss SIGMA (Carl Zeiss AG, Oberkochen, Germany). High-resolution transmission electron microscope (HRTEM) images were obtained using a Tecnai G3 F30 S-TWIN (FEI, Hillsboro, USA). Samples were supported on Ultra-thin carbon film. Nanoscale chemical composition analyses were carried out simultaneously. X-ray photoelectron spectroscopy (XPS) was performed using a non-monochromatic Thermo ESCALAB 250Xi X spectrometer (Thermo Fisher Scientific, Massachusetts, USA) to generate Al Kα radiation ($hv = 1486.6$ eV) (10−10 Torr) under ultra-high vacuum. The charging effect is corrected relative to the carbon peak C 1s (284.8 eV). The deconvolution of the peak spectrum is performed by XPSPEAK41 software, using Gaussian–Lorentzian linear and Shirley background subtraction. The Brunauer-Emmett-Teller (BET) is measured by a nitrogen physical adsorption (ASAP 2460 Micrometrics). The liquid product was quantified by ^{1}H NMR using the internal standard method (DMSO as the internal standard and D_2O as the solvent) by a 600 MHz nuclear magnetic resonance spectrometer (Bruker AVANCE NEO 600). The spent catalyst was characterized after the catalyst surface was washed with pure water, and ultrasound was used for backup.

Electrochemical measurements. To prepare the Cu_xCo_y-BTC, 2 mg powder was suspended in the ink dispersion (500 μL H_2O, 500 μL isopropanol and 40 μL Nafion) to form a homogeneous ink by ultrasonication. Then, the ink was dropped evenly on the CP (1.0 cm ×

1.0 cm) surface, followed by drying under the infrared lamp. Electrochemical measurement was performed by the CHI660e electrochemical workstation. In a three-electrode system, the catalyst was loaded onto 1.0 cm × 1.0 cm carbon paper as the working electrode, Hg/HgO electrode as the reference electrode, and 1.0 cm × 1.0 cm Pt sheet electrode as the opposite pole, performance tests were performed in different concentrations of KOH and methanol and ethanol electrolytes (as specified in the respective figure captions). All polarization tests were performed via linear sweep voltammetry (LSV) at 50 mV s^{-1}. Moreover, the long-term stability of the catalysts was estimated via the multi-current step. For NMR analysis, usually 600 μL electrolyte is mixed with 60 μL D_2O and 2 μL DMSO, where DMSO is the internal standard. Faraday efficiency (FE) was calculated according to the following calibration curve: $FE = \frac{mnF}{J\,S\,t}$, where n is the total number of electrons transferred by the product (Ethanol to acetate usually transfers 4 electrons, and methanol to formate usually transfers 4 electrons, $FE = \frac{4mF}{J\,S\,t}$), m is the actual number of moles of ethyl acetate generated (mol), F is the Faraday constant (96485 C/mol), j is the current density (mA cm^{-2}), S is the catalyst area (cm^2) and t is time (s).

Supplementary Figures and Tables

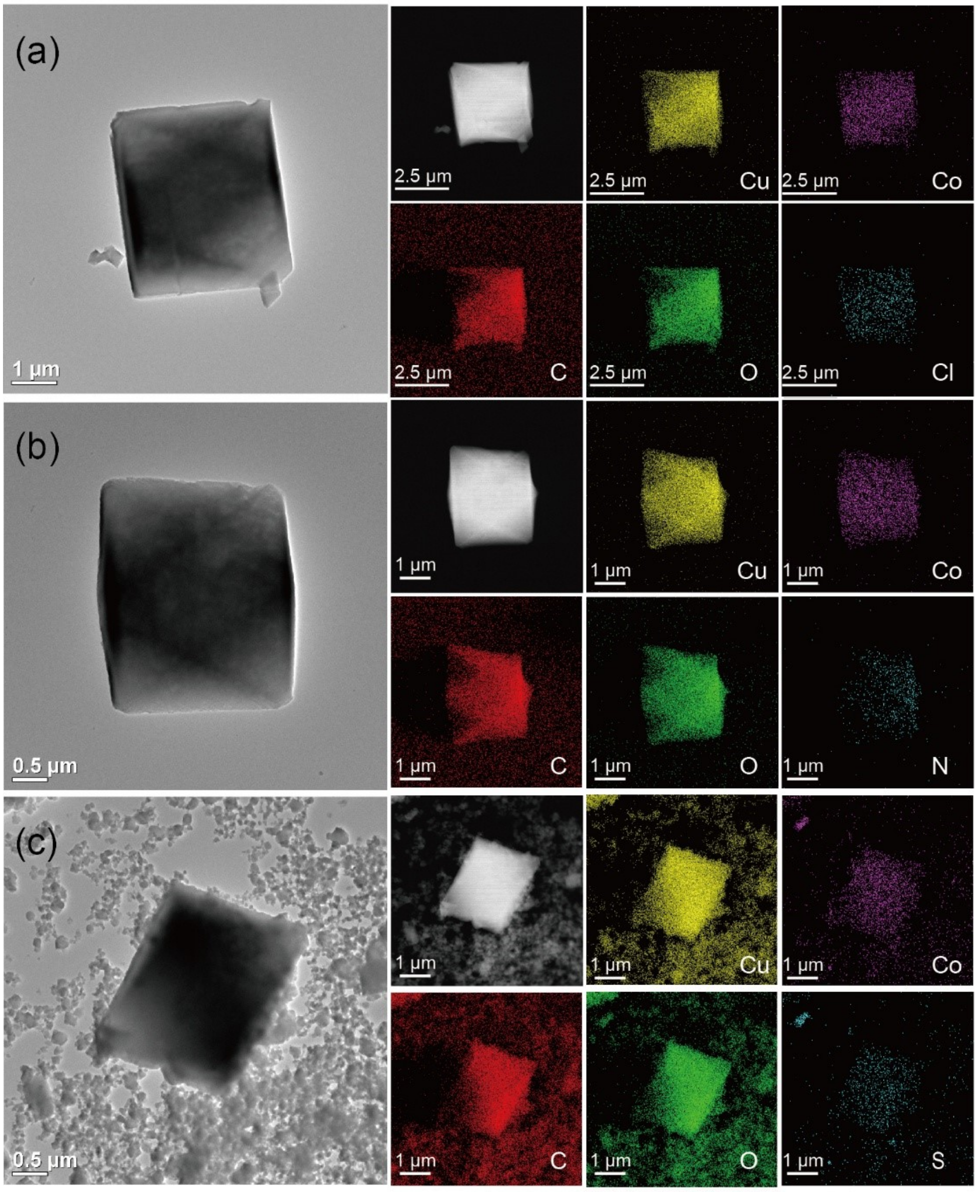

Fig. S1 TEM images and HAADF-STEM images of (a) Cl^-, (b) NO_3^-, (c) SO_4^{2-} of different anionic sources $Cu_{0.4}Co_{0.6}$-BTC materials, including elemental mappings of C, Cu, Co and O elements, which are evenly distributed throughout the material.

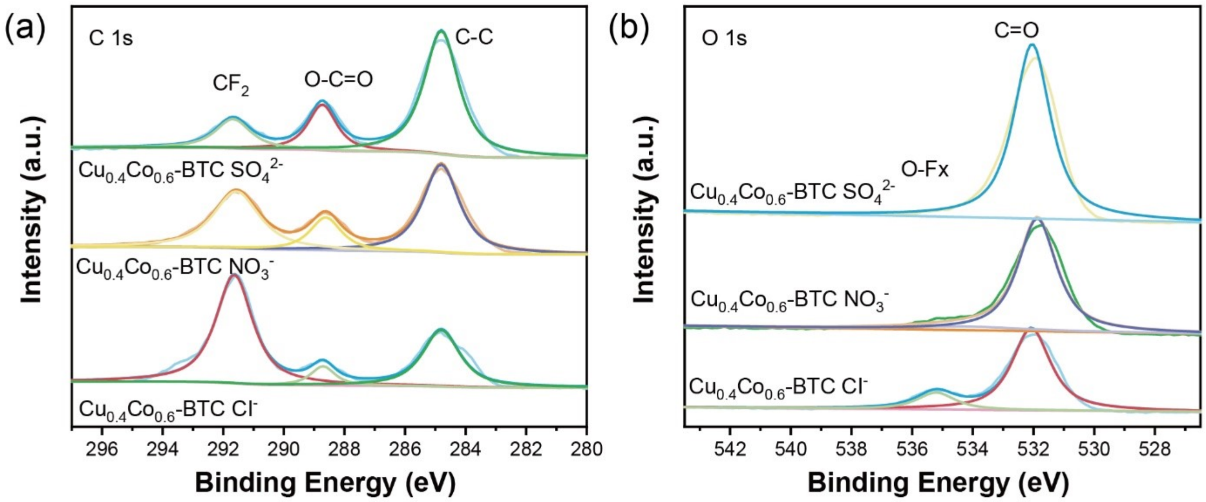

Fig. S2 XPS characterization of Cu$_{0.4}$Co$_{0.6}$-BTC materials prepared with different anion sources: (a) C 1s spectrum and (b) O 1s spectrum.

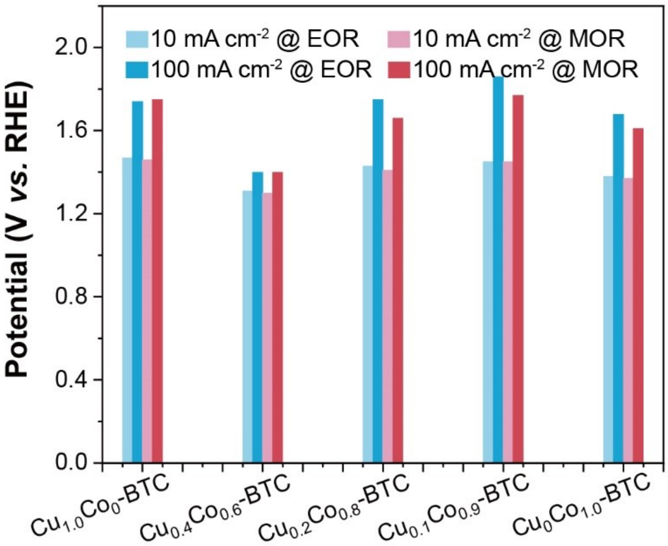

Fig. S3 The electrocatalytic performance evaluation over $Cu_{0.4}Co_{0.6}$-BTC (SO_4^{2-}): Corresponding potentials of Cu_xCo_y-BTC (SO_4^{2-}) under different Cu/Co ratios at 10 mA/cm^{-2} and 100 mA/cm^{-2} for EOR and MOR, respectively.

Supplementary Note: A series of variable component Cu_xCo_y-BTC materials were synthesized by changing the Cu/Co bimetallic ratio, and the electrocatalytic alcohol oxidation potential was compared at the current density of 10 mA cm^{-2} and 100 mA cm^{-2}, and the catalytic performance was evaluated in more detail. The results show that when the Cu/Co ratio is 0.4/0.6, the oxidation potential of alcohol is 1.31 V *vs.* RHE (EOR at 10 mA cm^{-2}), 1.3 V *vs.* RHE (MOR at 10 mA cm^{-2}), 1.4 V *vs.* RHE (EOR at 100 mA cm^{-2}), 1.4 V *vs.* RHE (MOR at 100 mA cm^{-2}), respectively. When the current density is 100 mA cm^{-2}, the AOR (both EOR and MOR) potential is reduced by 190 mV compared with the OER potential. It is proved that the Cu/Co ratio of 0.4/0.6 is more favorable for EOR and MOR than other loading ratios, which may be due to the optimum synergistic effect between metals and the unique metal-support interaction between metals and ligands affecting the catalytic oxidation of alcohols.

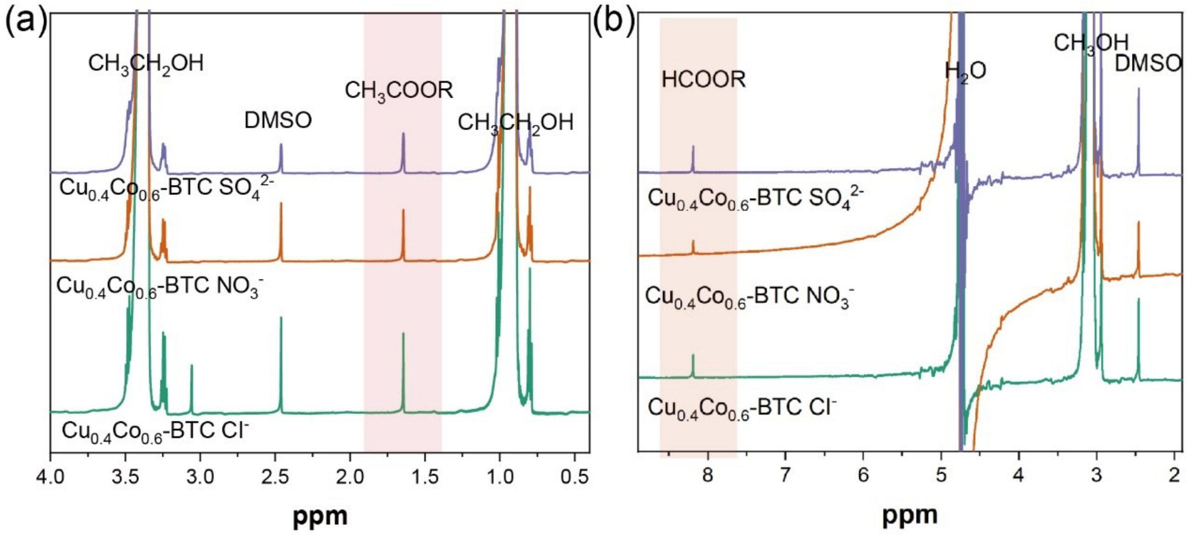

Fig. S4 ^{1}H NMR spectra of bulk electrolysis for 1h at different current densities over $Cu_{0.4}Co_{0.6}$-BTC (SO_4^{2-}) electrocatalysts for (a) EOR and (b) MOR. For EOR, the singlet state with a chemical shift of about 1.65 ppm is the methyl group near the carboxyl group in acetate. For MOR, the singlet state with a chemical shift of about 8.2 ppm is the hydrogen near the carboxyl group in the formate ester.

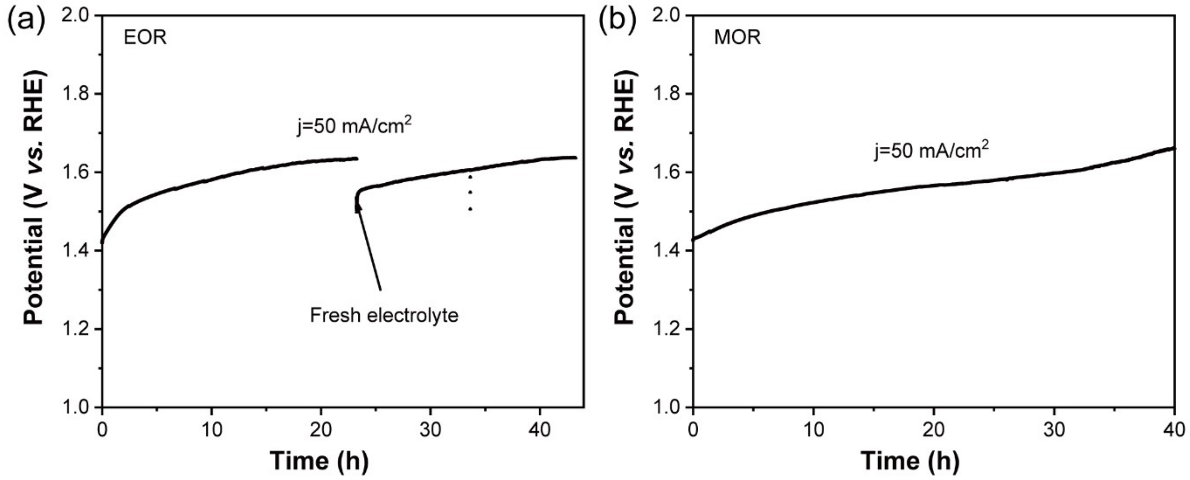

Fig. S5 The long-term stability evaluation over $Cu_{0.4}Co_{0.6}$-BTC (SO_4^{2-}) for (a) EOR and (b) MOR system at 50 mA cm^{-2} by multi-current steps.

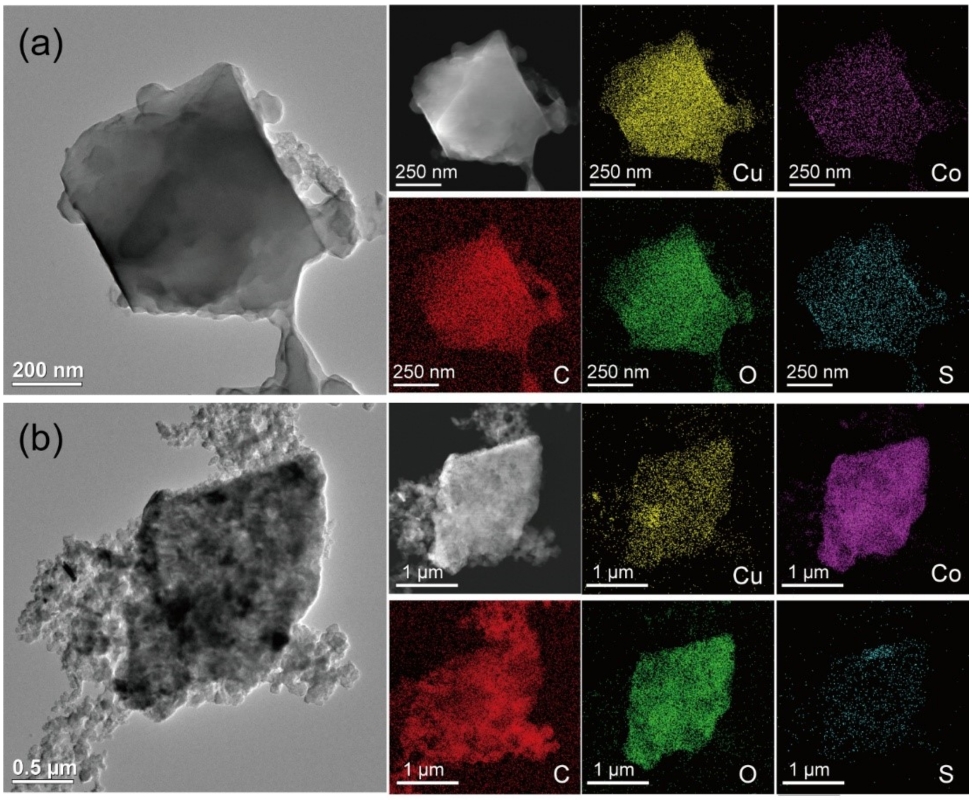

Fig. S6 TEM images and HAADF-STEM images of $Cu_{0.4}Co_{0.6}$-BTC (SO_4^{2-}) after (a) EOR and (b) MOR, including elemental mappings of C, Cu, Co, O, and S elements, which are evenly distributed throughout the material.

Table S1. Content of the main elements (Cu, Co, C, O) and anion elements (Cl, N, S) in $Cu_{0.4}Co_{0.6}$-BTC (Cl^-, NO_3^-, SO_4^{2-}) materials with different anion sources as determined by TEM mapping.

Elements	**$Cu_{0.4}Co_{0.6}$-BTC Cl^- (wt%)**	**$Cu_{0.4}Co_{0.6}$-BTC NO_3^- (wt%)**	**$Cu_{0.4}Co_{0.6}$-BTC SO_4^{2-} (wt%)**
C	29.91	32.53	34.67
O	17.98	19.78	21.9
Co	2.19	2.09	1.09
Cu	49.71	45.6	42.2
anion elements	0.20 (Cl)	0 (N)	0.14 (S)

Table S2. Summary N_2-physisorption data of different anionic sources $Cu_{0.4}Co_{0.6}$-BTC

Catalysts	**S_{BET} (m^2/g)**	**Vt (cm^3/g)**	**Av. particle size (µm)**
$Cu_{0.4}Co_{0.6}$-BTC Cl^-	1019	0.52	~6
$Cu_{0.4}Co_{0.6}$-BTC NO_3^-	972	0.52	~5.5
$Cu_{0.4}Co_{0.6}$-BTC SO_4^{2-}	462	0.35	~3

materials

Table S3. Analyze the peak area of Co elements in XPS

Catalysts	**Co^{3+} $2p_{3/2}$**	**Co^{2+} $2p_{3/2}$**	**Co^{3+} $2p_{1/2}$**	**Co^{2+} $2p_{1/2}$**
$Cu_{0.4}Co_{0.6}$-BTC SO_4^{2-}	1643	1880	439	1061
$Cu_{0.4}Co_{0.6}$-BTC NO_3^{-}	1114	890	590	0
$Cu_{0.4}Co_{0.6}$-BTC Cl^{-}	727	660	554	0

[1] Y. Li, X. Gong, A. Dutta Chowdhury, Toward Developing Superior Cu-Based Metal-Organic Framework-Derived Materials for Electrocatalytic Oxidation of Ethanol, Inorg. Chem. 63 (2024) 11258–11269.

[2] Y. Li, X. Gong, L. Gu, A. Dutta Chowdhury, Evaluating the efficiency of CuCo-based metal-organic framework-derived materials for electrocatalytic oxidation of alcohols, Mater. Today Chem. 36 (2024) 101961.

[3] T. Wang, H.K. Kim, Y. Liu, W. Li, J.T. Griffiths, Y. Wu, S. Laha, K.D. Fong, F. Podjaski, C. Yun, R.V. Kumar, B. V. Lotsch, A.K. Cheetham, S.K. Smoukov, Bottom-up Formation of Carbon-Based Structures with Multilevel Hierarchy from MOF-Guest Polyhedra, J. Am. Chem. Soc. 140 (2018) 6130–6136.

[4] S.S.Y. Chui, S.M.F. Lo, J.P.H. Charmant, A.G. Orpen, I.D. Williams, A chemically functionalizable nanoporous material [Cu3(TMA)2 (H2O)3](n), Science (80-.). 283 (1999) 1148–1150.

[5] Y. Li, A.D. Chowdhury, Exploring Electrocatalytic CO2 Reduction Over Materials Derived from Cu-Based Metal-Organic Frameworks, ChemCatChem. 0 (2024) e202401551.